Bulletin of Mathematical Biology manuscript No.
(will be inserted by the editor)

Appendices to: The signature of endemic populations in the spread of mountain pine beetle outbreaks

Dean Koch · Mark A. Lewis · Subhash Lele

Received: date / Accepted: date

1 Datasets

1.1 Host density $\boldsymbol{H}$

Host density $H_{i,t}$, or the number of susceptible overstory pine trees within the 1 ha square of land in cell i in year t, was approximated using variable $h_{i,t}$, the combined above-ground biomass at cell i attributed to *Pinus* species. We calculated this from a 2001 baseline estimate supplied in Beaudoin et al. (2014), making adjustments in each subsequent year by subtracting losses from wildfire and logging (using data from http://www.hectaresbc.org), as well as MPB.

While raw data in units of live mature stems/ha would be both more realistic and convenient, they are typically not available at the scale and resolution that we are interested in. We therefore simply rescaled h_i to match empirical distributions of H_i based on ground surveys (Figure 1).

In a 2006 survey of 28 high-density stands in the Merritt TSA by Nigh et al. (2008), the highest observed density was 2810 stems/ha, 92% of which was pine. Based on that maximum we assigned a scaling factor of $s_h = 0.92 \times 2810/\max_i(h_{i,2006}) = 9.1$ and fixed $H_{i,t} = s_h h_{i,t}$. A more cautious approach, for example using mensurational

Dean Koch is postodoctoral fellow in the Department of Mathematical and Statistical Sciences, University of Alberta (UofA), Edmonton, Canada T6G 2R3 (email: dkoch@ualberta.ca, ORCID: https://orcid.org/0000-0002-8849-859X); Subhash R. Lele is Professor of Mathematical and Statistical Sciences at UofA (email: slele@ualberta.ca); Mark A. Lewis (MAL) is Professor of Mathematical and Statistical Sciences and Biological Sciences at UofA (email: mark.lewis@ualberta.ca, ORCID: https://orcid.org/0000-0002-7155-7426). The authors thank the Lewis Research Group for providing expert advice and feedback, as well as Victor Shegelski and the Sperling Lab for providing flight mill data. MAL is also grateful for support through NSERC and the Canada Research Chair Program.

Dean Koch, Mark A. Lewis, and Subhash Lele
Department of Mathematical and Statistical Sciences, University of Alberta, 11324 89 Ave NW, Edmonton, AB, T6G 2J5, Canada.
E-mail: dkoch@ualberta.ca, mlewis@ualberta.ca, slele@ualberta.ca

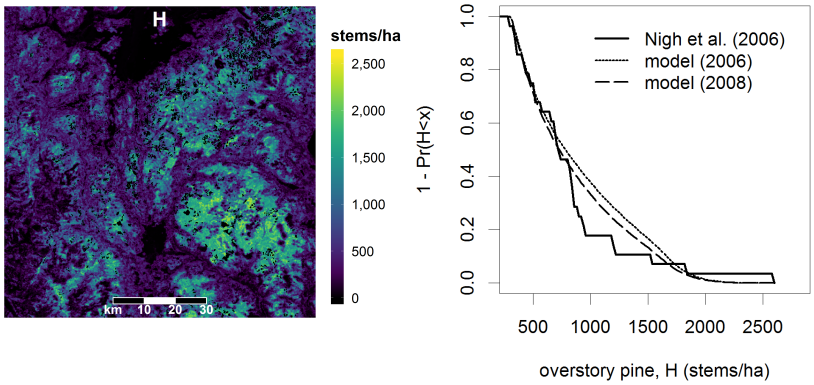

Fig. 1: Heatmap of host density $H_{i,t} = s_h h_{i,t}$, estimated from rescaled pine volume data $h_{i,t}$. At right, the empirical CDF of pre-attack host density in 2006 and 2008 (dashed and dotted lines) are compared against an overstory pine density survey from 2006 by Nigh et al. (2008) (solid line).

projections for the stands in our study area, is possible but was avoided for the sake of simplicity. However our linear rescaling produced a reasonably close agreement in empirical cumulative distribution (CDF) functions (Figure 1), and the scaling factor of $\approx 10X$ is essentially a linearization of the more carefully constructed nonlinear volume-density curve derived in Goodsman et al. (2016) (Appendix S1).

1.2 Pine mortality $\boldsymbol{\phi}$

Our response variable $\phi_{i,t}$ is the percent of $H_{i,t}$ killed by pine beetle attack in the summer of year t. We derived these values from AOS data comprising two types of GIS information collected annually by BC's provincial forest management agency: polygons with categorical damage severity attributes (digitized sketch maps) indicating large contiguous areas of infestation; and spot data indicating a small cluster of infested stems at a particular location. Because crown-fade typically happens with a one-year delay, we refer to year $t + 1$ in the AOS dataset as the *attack year* t.

To convert polygons to raster format we followed a protocol introduced by Chen and Walton (2011); the five AOS damage severity categories (corresponding to intervals of percent mortality: trace <1%, light 1-10%, moderate 11-29%, severe 30-49%, very severe >50%) were interpreted by multiplying the midpoint of each interval with the percent area of overlap with each cell. Spots were interpreted by defining a quarter-hectare circle centered at the point coordinates and assigning it a 30% mortality value (reflecting AOS-wide average stand loading and spot infestation levels).

Some minor modifications of these mortality data were needed to correct obvious positional errors and to make our analysis approach feasible: Attack rates >1 (due to multiple overlapping damage observations) were truncated to one, and values at

locations unsuitable for MPB (water bodies, non-treed areas, *etc.*) were set to zero. We then added the small constant $\xi = 4 \times 10^{-6}$ (equal to one half the minimum finite logit value) to each cell before dividing by $1 + \xi$. This ensured that $0 < \phi_i < 1$, so that $\text{logit}(\phi_i)$ is defineable all sites. It is also consistent with premise of ubiquitous endemic MPB populations, undetectable by the AOS (Wulder et al. 2006).

1.3 Stand susceptibility covariates

Beetle pressure is only part of the equation in MPB attack dynamics. Environmental conditions before and during an attack, as well as the density, composition, and health of the stand influence the ability of a given pine to resist bark beetle attack (Taylor et al. 2006; Nelson et al. 2008). These local conditions are often summarized as *stand susceptibility*, a ranking of relative risk (to MPB attack) computed from local covariates. The model of Shore et al. (2000), for example, uses the product of four covariates relating to: pine dominance; stand density; stand age; and elevation.

Our model uses a similar product of stand characteristics along with a suite of additional microclimate and topography-related covariates, similar to those found in Aukema et al. (2008). Local stand characteristics, such as H_i, were derived from the Beaudoin et al. (2014) model, and topographical features were drawn from provincial government datasets (http://www.hectaresbc.org). Local weather variables, such as temperature and precipitation highs/lows were constructed using the *climateBC* model, via elevation-adjusted extrapolations from weather station measurements and climatic norms (Spittlehouse 2006). In total, we compiled 43 such covariates for each of the n sites in the study area ($n_\beta = 44$, including an intercept). These are the rows of the $n \times n_\beta$ matrices $\boldsymbol{X}_t$. They are summarized in Table 1.

2 Redistribution kernels for 2-dimensional space

Redistribution kernels view dispersal events as moving individuals from a fixed source to a random destination. If the coordinates of the i^{th} possible destination are $\boldsymbol{s}_i = (x_i, y_i)'$, then we write the *movement vector* from source (j) to destination (i) as $\boldsymbol{\delta}_{ij} = \boldsymbol{s}_i - \boldsymbol{s}_j = (\delta^x_{ij}, \delta^y_{ij})'$, where $\delta^x_{ij} = x_i - x_j$ and $\delta^y_{ij} = y_i - y_j$ are the components of the movement along the x and y axes. Direction (angle α_{ij}) and distance (d_{ij}) are then given by the identities $d^2_{ij} = |\boldsymbol{\delta}_{ij}|^2 = (\delta^x_{ij})^2 + (\delta^y_{ij})^2$, and $\tan(\alpha_{ij}) = \delta^y_{ij}/\delta^x_{ij}$.

We define the redistribution kernel $D(\boldsymbol{s}_i, \boldsymbol{s}_j; \boldsymbol{\Delta})$ to be the probability mass function (PMF) for possible destinations, with parameters $\boldsymbol{\Delta}$. For simplicity modelers usually choose kernels that are spatially *stationary* (invariant to location), and *isotropic* (invariant to direction). Stationarity means movement probabilities depend only on direction and distance, so D can be written $D(\boldsymbol{\delta}_{ij}; \boldsymbol{\Delta})$. With the additional assumption of isotropy, D becomes a function of distance d_{ij} only, or $D = D(d_{ij}; \boldsymbol{\Delta})$. In general, we will write D for the function and $[D]_{ij}$ for its value with source j and destination i.

The (isotropic and stationary) Gaussian is the most common kernel in applications:

$$D_G(d_{ij}; \rho) = c \exp\left(-d^2_{ij}/\rho\right), \text{ where } d_{ij} = |\boldsymbol{s}_i - \boldsymbol{s}_j|. \tag{1}$$

Category	Name	Units	Source
topography	altitude	m above sea level	provincial topography layers from hectaresbc.org (accessed 06/2019)
	slope	° above horizontal	
	aspect	° from true north	
	lakes indicator	binary	
stand inventory	treed area	%	damage-adjusted estimates from Beaudoin et al. (2014) based on remotely-sensed data from 2001 (see Section 1.1)
	stand age	years	
	pine density	stems/ha	
	log pine density	log(stems/ha)	
beetle activity	lagged pine mortality	%	ϕ_t and $\phi_t H_t$ lagged by one and two years (see Sections 1.2-1.1)
	lagged infested stems	stems/ha	
temperature	minima	°C	All climatic variables are seasonal, with separate covariates for: autumn of year $t-1$; winter, spring, and summer of year t. These are estimated using climateBC software from (Spittlehouse 2006).
	averages	°C	
	maxima	°C	
cooling days	days below 0°C	°C · days	
	days below 18°C	°C · days	
warming days	days above 5°C	°C · days	
	days above 18°C	°C · days	
precipitation	totals	mm / 4 months	

Table 1: The 43 covariates included in the linear regression model for stand susceptibility. 31 of these are climatic (four seasons × 8 factors, with the exclusion of degree days above 18° to avoid collinearity problems); Four are lagged state variables (pine mortality and infested stem counts, lagged by one and two years); Four describe the local host population; and four are topographical.

c is a normalization constant, chosen such that with $\boldsymbol{s}_j$ fixed, the summation of (1) over all destinations is equal to one. This normalization is a general requirement of any PMF, but in the context of redistribution kernels it ensures that total population counts are conserved. More precisely, if we start from local source populations of size $\tilde{B}_j$, with individuals at each source dispersing independently and according to D, then the expected number to arrive at destination i is $B_i = \sum_j [D]_{ij} \tilde{B}_j$, and the sum of the B_i is equal to the sum of the source populations.

Thus D is sometimes chosen by selecting a function that matches the profile of empirical data on B_i. Other times, hypotheses about the movement mechanism lead to mathematical derivations. For example, under a quite general set of circumstances, diffusion through 2D space gives rise to the WMY kernel family (Yasuda 1975; Yamamura 2002; Hapca et al. 2009):

$$D_W\left(d_{ij}; \boldsymbol{\Delta}_W\right) = c\left(d_{ij}/\rho\right)^{\nu} K_\nu\left(d_{ij}/\rho\right), \text{ where } \boldsymbol{\Delta}_W = (\nu, \rho)', \tag{2}$$

with shape parameter $\nu > -1$; range parameter $\rho > 0$; normalization constant c (computed as above); and with K_ν to denote the ν^{th} order modified Bessel function of the second kind.

The Gaussian (1) and 2D Laplace kernels used in Heavilin and Powell (2008), are limiting/special cases of the WMY ($\nu \to \infty$, and $\nu = 1/2$, respectively). The Bessel kernel appearing in the bark beetle models of Turchin and Thoeny (1993) and

Goodsman et al. (2016) is another special case ($\nu = 0$). In this sense (2) is robust with respect to hypotheses about movement. We use an approximation to (2) that is somewhat more flexible, the geometrically anisotropic product-WMY:

$$D_{\otimes}\left(\boldsymbol{\delta}_{ij};\boldsymbol{\Delta}\right) = cD_W\left(d_{ij}^x;\boldsymbol{\Delta}^x\right)D_W\left(d_{ij}^y;\boldsymbol{\Delta}^y\right), \quad \text{with } \boldsymbol{\Delta} = (\alpha,\boldsymbol{\Delta}^x,\boldsymbol{\Delta}^y)', \text{ and } (d_{ij}^x,d_{ij}^y)' = \boldsymbol{R}_\alpha\boldsymbol{\delta}_{ij}, \tag{3}$$

where $\boldsymbol{R}_\alpha$ is the standard 2D rotation matrix for angle α and c the normalization constant. This kernel is similar to the WMY, closely approximating it over much of its parameter range, yet it can be computed far more quickly because, like the Gaussian, it is spatially separable (Koch et al. 2020b). Moreover it better captures directed movements, by means of angle α and the independent shape/range parameter sets, $\boldsymbol{\Delta}^x$ and $\boldsymbol{\Delta}^y$, representing two orthogonal directions. Thus unlike an isotropic kernel, (3) captures ellipsoid patterns of redistribution (see Figure 3 of main text).

Our nonstationary formulation of D uses a weighted combination of $m = 625$ stationary kernels $D_{\otimes_k}$ $(k = 1\ldots m)$, each of the form (3), and each with its own parameter set $\boldsymbol{\Delta}_k$. Each is spatially referenced, with coordinates $\boldsymbol{r}_k$ to denote the centroid of a 10×10 km block over which $D_{\otimes_k}$ is assumed to reasonably approximate local flight patterns. The predictions of these local kernels are combined by weighted averaging, with weights inversely related to distance from the centroid $\boldsymbol{r}_k$ to the prediction site $\boldsymbol{s}_i$. For a given weighting function $\omega(d)$, we define the nonstationary kernel:

$$D(\boldsymbol{s}_i,\boldsymbol{s}_j;\boldsymbol{\theta}_D) = c_j\sum_{k=1}^{m}\omega\left(|\boldsymbol{s}_i-\boldsymbol{r}_k|\right)D_{\otimes_k}\left(\boldsymbol{s}_i-\boldsymbol{s}_j;\boldsymbol{\Delta}_k\right), \text{ where } \boldsymbol{\theta}_D = (\boldsymbol{\Delta}_1,\ldots,\boldsymbol{\Delta}_m)' \tag{4}$$

where the (source-dependent) normalization constant c_j is computed as the reciprocal of the sum of (4) over all i (with c_j set to 1 in this calculation), ensuring that density is preserved.

We used a bisquare weighting function $\omega(d) = \lceil 1-(d/r)^2\rceil^2$, with the ceiling function $\lceil x\rceil$ enforcing a cutoff distance of $r = 7.1$ km beyond which zero weight is assigned. Centroids $\boldsymbol{r}_k$ were arranged in a 25×25 grid of overlapping blocks, with a spacing of 3.3 km between centroids. This balanced a need for large samples within each block (10×10 km $= 10^4$ points) and high resolution estimates of $\mathbb{E}(\boldsymbol{B}_t)$.

3 Model-fitting and simulations

Covariograms are in many ways similar to redistribution kenels. We use a geometrically anisotropic Gaussian covariogram, which defines the covariance between errors at $\boldsymbol{s}_i$ and $\boldsymbol{s}_j$ to be:

$$[\boldsymbol{V}_t]_{ij} = \mathrm{Cov}\left(Z_{i,t},Z_{j,t}\right) = \sigma_t^2\exp\left((d_x)^2/\rho_x\right)\exp\left((d_{ij}^y)^2/\rho_y\right), \tag{5}$$

where $(d_x,d_y)' = \boldsymbol{R}_\alpha|\boldsymbol{s}_i-\boldsymbol{s}_j|$

with $\rho_x, \rho_y > 0$ the range parameters, and α the angle of orientation. For reasons of computational efficiency we fixed $\alpha = 0$ so that (5) remains spatially separable (Koch et al. 2020a).

3.1 Estimation

Supposing beetle pressure is known – either by direct measurement, or by fixing biologically reasonable values for ϵ_t and $\boldsymbol{\theta}_{D_t}$ – then equation (5) of the main text will become linear in the remaining attack dynamics parameters κ_t and $\boldsymbol{\beta}_t$. The maximization problem in equation (6) of the main text then becomes a spatial linear regression on stand susceptibility, much like in Aukema et al. (2008) and Zhu et al. (2010) except with an explicit (rather than implicit) error model. In this situation, using generalized least squares (GLS), it is straightforward to find $\hat{\boldsymbol{\theta}}_{\phi_t}$ and $\hat{\boldsymbol{\theta}}_{V_t}$ numerically using a 2-step estimator (Chilès and Delfiner 2012).

Similarly if $\boldsymbol{\theta}_{D_t}$, but not $\boldsymbol{\theta}_{\phi_t}$, is known, it remains a relatively straightforward 1-dimensional optimization problem to find $\hat{\boldsymbol{\theta}}_{\phi_t}$ and $\hat{\boldsymbol{\theta}}_{V_t}$ by profile likelihood on ϵ using GLS as above (Crujeiras and Van Keilegom 2010). However with all three components unknown, the inference problem is far more involved. Our solution is three stage algorithm that requires an initial estimate of beetle pressure. We used $\epsilon = 0$ and the stationary Bessel kernel reported in Goodsman et al. (2016):

1. Assume $\boldsymbol{V}_t \propto \boldsymbol{I}$. Estimate $\hat{\boldsymbol{\beta}}_t$ and $\hat{\sigma}_t$ by OLS given the initial beetle pressure values. Estimate $\hat{D}_t$ by blockwise MLE given $\boldsymbol{\beta} = \hat{\boldsymbol{\beta}}_t$. Estimate $\hat{\boldsymbol{\theta}}_{\phi_t}$ by profile likelihood on ϵ given $D_t = \hat{D}_t$.
2. Estimate $\hat{\boldsymbol{\theta}}_{V_t}$ by MLE on the model residuals from stage 1. Refine the estimate of $\hat{\boldsymbol{\theta}}_{\phi_t}$ by profile likelihood on ϵ given $D_t = \hat{D}_t$.
3. Assume $\boldsymbol{\theta}_{V_t} = \hat{\boldsymbol{\theta}}_{V_t}$. Refine the estimate of $\hat{D}_t$ by blockwise MLE given $\boldsymbol{\beta} = \hat{\boldsymbol{\beta}}_t$ from stage 2. Refine the estimate of $\hat{\boldsymbol{\theta}}_{\phi_t}$ by profile likelihood on ϵ given $D_t = \hat{D}_t$.

In stages 1 and 3, "blockwise MLE" for $\hat{D}_t$ means the following: we split the dataset into square blocks (each containing 10^4 locations) centered over the 625 points of a 25×25 evenly spaced grid covering the study area, and assigned a pWMY kernel (with parameters $\boldsymbol{\Delta}_{k,t}$) to each one. Fixing $\boldsymbol{\beta}_t$ and $\boldsymbol{V}_t$ to their most current estimates as specified in stages 1/3, for each block we jointly estimated the seven remaining unknown parameters (ϵ, κ, and $\boldsymbol{\Delta}_{k,t}$) by numerically maximimizing the likelihood function in equation (6) of the main text, under the assumption that D_t is the stationary kernel (3) with parameters $\boldsymbol{\Delta}_{k,t}$. We then used the $\hat{\boldsymbol{\Delta}}_{k,t}$ to construct D_t using (4) (discarding the local estimates of ϵ and κ).

3.2 Simulations

Our 3-stage algorithm is similar to one described by Crujeiras and Van Keilegom (2010), where $\hat{\boldsymbol{\theta}}_{\phi_t}$ and $\hat{\boldsymbol{\theta}}_{D_t}$ are jointly estimated and $\hat{\boldsymbol{\theta}}_t$ is known to be asymptotically normal and unbiased. However since ours estimates $\hat{\boldsymbol{\theta}}_{\phi_t}$ and $\hat{\boldsymbol{\theta}}_{D_t}$ separately, we have no theoretical guarantees of its large-sample properties. Instead we investigated the properties of our estimators in simulations.

Since our model is computationally intensive, we conducted simulations on a smaller spatial scale – 33×33 km, covered by a 5×5 layout of blocks – and generated D_t using anisotropic Gaussian (instead of pWMY) kernels. The fitted model, however, was as described in the main text, using pWMY kernels to fit D_t. In each of 100 repetitions, we assigned values to the parameters in Table 2 (of the main text) uniformly at random within a biologically reasonable range – *e.g.* $0.1 < \kappa < 25$, $1 < \epsilon < 500$, and $25 < \lambda < 1000$ – and used covariate data pulled from a randomly located subset of the full 2008 data. We then used equation (5) of the main text to compute the true response values $\text{logit}(\boldsymbol{\phi})$, adding them to randomly generated MVN errors $\boldsymbol{Z}_t$ to produce a (simulated) observed response.

The response and associated covariates were fed into the algorithm of Appendix 3.1 to yield estimates $\hat{\boldsymbol{\theta}}_t$ separately for each repetition. Errors in estimation for the attack parameters $\boldsymbol{\theta}_{\phi_t}$ and the angles of anisotropy $\alpha_{k,t}$ are summarized in Figure 2. For comparison we also report the errors after stage 1, where the $\boldsymbol{Z}_t$ are assumed to be indepedendent in space (a model misspecification).

Raster plots of the estimated post-flight MPB density closely approximated the true (simulated) ones. Individual fitted stationary kernels also closely resembled the true ones, favouring large shape values (and thus approximating the Gaussian closely), and estimating the dispersal orientation angles with remarkable precision. Interestingly the autocorrelation correction (stages 2-3) had little impact on these angle estimates, so although beetle density estimates differed slightly between stages 1 and 3, the error distribution of the $\alpha_{k,t}$ appears largely unchanged (Figure 2).

However the results for the other parameters highlight some of the reasons we must not ignore spatial autocorrelation: uncertainty is underestimated under an incorrect independence assumption, leading to a wider than expected spread of errors and more frequent misspecifications of $\hat{\alpha}_{i,t}$. In our case, this imprecision appeared to introduce bias in the more sensitive components of the model; Both ϵ and κ tended to be underestimated in stage 1. The stage 3 autocorrelation correction appears to largely eliminate this bias and improve precision (peakedness of the density plots).

The error distributions of the individual $\hat{\beta}_{k,t}$ showed good agreement with the large sample asymptoptic theory in Crujeiras and Van Keilegom (2010), from which confidence intervals can be computed by inverting the Fisher information matrix corresponding to equation (6) of the main text. Uncertainty in the distributions for ϵ and κ, however, was underestimated by this theory; with only 38% (and 42%, respectively) of estimates lying inside their nominal 95% intervals. This may be due to an inadequate sample size, or a failure to find the values of $\hat{\boldsymbol{\theta}}_{\phi_t}$ and $\hat{\boldsymbol{\theta}}_{D_t}$ that *jointly* maximize the full likelihood in stages 1 and/or 3. We therefore omit confidence intervals for these parameters in the main text, reporting the $\hat{\epsilon}$ and $\hat{\kappa}$ simply as point estimates.

References

Aukema BH, Carroll AL, Zheng Y, Zhu J, Raffa KF, Dan Moore R, Stahl K, Taylor SW (2008) Movement of outbreak populations of mountain pine beetle: Influences

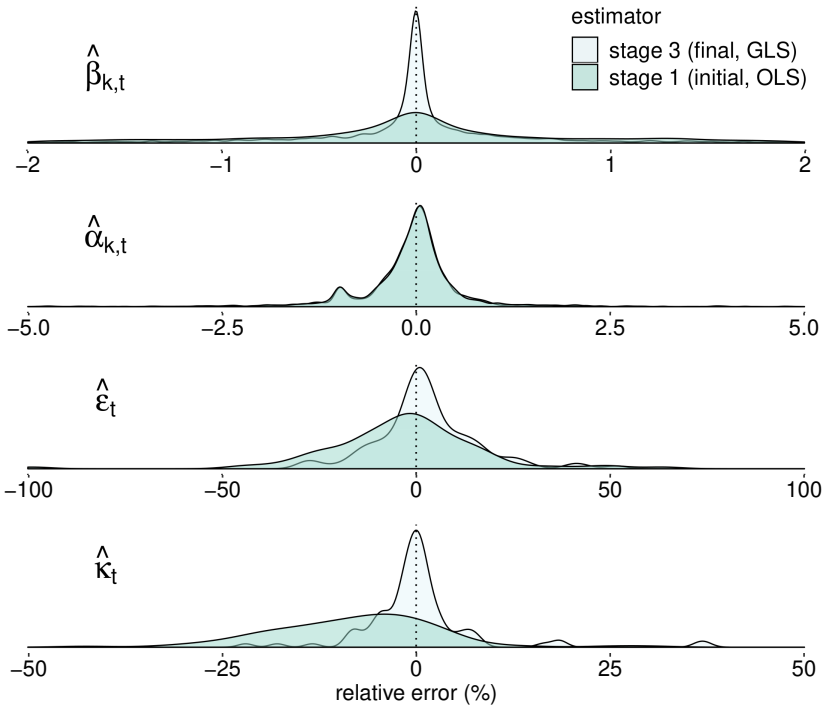

Fig. 2: Relative errors (discrepancy with exact values) in parameter estimation, using the 3-stage algorithm (Appendix 3.1) in 100 independent simulations (indexed by t). Results on 44 regression parameters ($\beta_{1,t} \ldots \beta_{44,t}$) and 25 angles of dispersal anisotropy ($\alpha_{1,t} \ldots \alpha_{25,t}$) are pooled and displayed as smoothed histograms. Stage 1 estimators ignore autocorrelation. Stage 3 estimators correct for it.

of spatiotemporal patterns and climate. Ecography (Cop) 31(3):348–358, DOI 10.1111/j.0906-7590.2007.05453.x

Beaudoin A, Bernier PY, Guindon L, Villemaire P, Guo XJ, Stinson G, Bergeron T, Magnussen S, Hall RJ (2014) Mapping attributes of Canada's forests at moderate resolution through kNN and MODIS imagery. Can J For Res 44(5):521–532, DOI 10.1139/cjfr-2013-0401

Chen H, Walton A (2011) Mountain pine beetle dispersal: spatiotemporal patterns and role in the spread and expansion of the present outbreak. Ecosphere 2(6):art66, DOI 10.1890/es10-00172.1

Chilès JP, Delfiner P (2012) Geostatistics: Modeling Spatial Uncertainty: Second Edition, vol 2. John Wiley & Sons, Hoboken, NJ, DOI 10.1002/9781118136188

Crujeiras RM, Van Keilegom I (2010) Least squares estimation of nonlinear spatial trends. Comput Stat Data Anal 54(2):452–465, DOI 10.1016/j.csda.2009.09.014

Goodsman DW, Koch D, Whitehouse C, Evenden ML, Cooke BJ, Lewis MA (2016) Aggregation and a strong Allee effect in a cooperative outbreak insect. Ecol Appl

26(8):2621–2634, DOI 10.1002/eap.1404

Hapca S, Crawford JW, Young IM (2009) Anomalous diffusion of heterogeneous populations characterized by normal diffusion at the individual level. J R Soc Interface 6(30):111–122, DOI 10.1098/rsif.2008.0261

Heavilin J, Powell J (2008) A novel method of fitting spatio-temporal models to data, with applications to the dynamics of mountain pine beetles. Nat Resour Model 21(4):489–524, DOI 10.1111/j.1939-7445.2008.00021.x

Koch D, Lele S, Lewis M (2020a) Computationally Simple Anisotropic Lattice Covariograms. Environ Ecol Stat DOI 10.1007/s10651-020-00456-2

Koch DC, Lewis MA, Lele SR (2020b) A unifying theory for two-dimensional spatial redistribution kernels with applications in population spread modelling. J R Soc Interface 17(170):20200434

Nelson WA, Potapov A, Lewis MA, Hundsdörfer AE, He F (2008) Balancing ecological complexity in predictive models: A reassessment of risk models in the mountain pine beetle system. J Appl Ecol 45(1):248–257, DOI 10.1111/j.1365-2664.2007.01374.x, URL http://doi.wiley.com/10.1111/j.1365-2664.2007.01374.x

Nigh GD, Antos JA, Parish R (2008) Density and distribution of advance regeneration in mountain pine beetle killed lodgepole pine stands of the Montane Spruce zone of southern British Columbia. Can J For Res 38(11):2826–2836, DOI 10.1139/X08-117

Shore TL, Safranyik L, Lemieux JP (2000) Susceptibility of lodgepole pine stands to the mountain pine beetle: Testing of a rating system. Can J For Res 30(1):44–49, DOI 10.1139/x99-182

Spittlehouse D (2006) ClimateBC: Your access to interpolated climate data for BC. Streamline Watershed Manag Bull 9(2):16–21

Taylor SW, Carroll AL, Alfaro RI, Safranyik L, Safranyik L, Wilson B (2006) The mountain pine beetle: A synthesis of biology. Canadian Forest Service, Victoria, BC, CA

Turchin P, Thoeny WT (1993) Quantifying dispersal of southern pine beetles with mark-recapture experiments and a diffusion model. Ecol Appl 3(1):187–198, DOI 10.2307/1941801

Wulder MA, Dymond CC, White JC, Leckie DG, Carroll AL (2006) Surveying mountain pine beetle damage of forests: A review of remote sensing opportunities. For Ecol Manage 221(1-3):27–41, DOI 10.1016/j.foreco.2005.09.021

Yamamura K (2002) Dispersal distance of heterogeneous populations. Popul Ecol 44(2):93–101, DOI 10.1007/s101440200011

Yasuda N (1975) The random walk model of human migration. Theor Popul Biol 7(2):156–167, DOI 10.1016/0040-5809(75)90011-8

Zhu J, Huang HC, Reyes PE (2010) On selection of spatial linear models for lattice data. J R Stat Soc Ser B Stat Methodol 72(3):389–402, DOI 10.1111/j.1467-9868.2010.00739.x